SSUKF-FA-RBF: A Kalman-Enhanced High-Precision Positioning Framework for BeiDou Navigation Using Firefly-Optimized Neural Estimation

Liang Li[1*], Shunli Hong[1], Xuexian Liu[2]
[1]School of Intelligent Transportation of Zhejiang Institute of Communications, Hangzhou 311112 China
[2]Zhejiang Highway and Water Transport Engineering Consulting Group Co., Ltd., Hangzhou 310000, China
E-mail: liliang@zjvtit.edu.cn
[*]Corresponding author

Keywords: beidou navigation system, inertial navigation, kalman filter algorithm, radial basis function neural network, firefly algorithm

Received: April 2, 2025

This study addresses the high-precision positioning requirements of the BeiDou Navigation System (BDS) by focusing on the commonly adopted BDS/Inertial Navigation System integrated navigation mode. A novel Spherical Simplex Unscented Kalman Filter (SSUKF) algorithm is proposed, featuring an improved sigma-point sampling strategy that enhances filtering accuracy while reducing computational overhead. In parallel, the Time Difference of Arrival (TDOA) method is combined with the Firefly Algorithm (FA) to optimize a Radial Basis Function (RBF) neural network, further enhancing positioning precision. Evaluation is conducted using an Ultra-Wideband TDOA dataset. Results show that the SSUKF algorithm significantly reduces positioning error. Specifically, the root means square error (RMSE) achieved by SSUKF is 0.1614 m-a reduction of 62.2% compared to the Extended Kalman Filter and 52.1% compared to the Unscented Kalman Filter. When integrated with the FA-optimized RBF neural network, the hybrid SSUKF-FA-RBF model achieves an RMSE of 0.127 m under high-noise conditions, demonstrating strong robustness and accuracy. In addition to its accuracy, the SSUKF algorithm offers improved computational efficiency, making it suitable for real-time, high-precision applications. Error analysis confirms the robustness and stability of the SSUKF-FA-RBF model across various environments. Under zero standard deviation noise, the model achieves 96.4% accuracy, 95.6% precision, and a 96.1% recall rate-substantially outperforming comparative models. This study contributes an enhanced Kalman filtering method and an optimized positioning framework, advancing both accuracy and computational efficiency for the BDS. The proposed approach offers effective technical support for a wide range of high-precision positioning applications.

Povzetek: Članek predstavi SSUKF-FA-RBF okvir, ki združuje izboljšani Kalmanov filter in ognjenooptimizirano RBF-nevronsko mrežo. Dosežek omogoča robustno in učinkovito pozicioniranje v sistemu BeiDou ter realnočasovne navigacijske aplikacije.

1 Introduction

With the rapid development of Global Navigation Satellite Systems (GNSS), the BeiDou Navigation System (BDS)-a satellite navigation system independently developed by China-plays a vital role in delivering high-precision positioning, timing, and navigation services [1]. However, limitations such as signal obstruction, error accumulation, and environmental interference restrict the standalone performance of BDS in terms of positioning accuracy [2]. To address this, integration with the Inertial Navigation System (INS) enables the complementary strengths of both systems, thereby improving overall accuracy and stability [3]. Nevertheless, traditional integrated navigation filters such as the Extended Kalman Filter (EKF) and Unscented Kalman Filter (UKF) often encounter limitations in nonlinear systems, including reduced accuracy and increased computational complexity. These challenges call for improved filtering algorithms [4, 5]. Concurrently, the Time Difference of Arrival (TDOA) method has emerged as a key approach for enhancing navigation accuracy, particularly due to its independence from additional synchronization signals and its suitability for complex environments [6]. However, TDOA performance is frequently degraded by noise, Non-Line-Of-Sight (NLOS) transmission, and convergence issues in traditional optimization techniques [7].

To overcome these limitations, this study proposes a Spherical Simplex Unscented Kalman Filter (SSUKF) algorithm that improves sigma-point sampling to enhance filtering accuracy and computational efficiency within the BDS/INS integration framework. Moreover, the study introduces a hybrid approach by combining TDOA with a Radial Basis Function (RBF) neural network optimized

using the Firefly Algorithm (FA). This design addresses the local optimum challenges associated with traditional gradient-based training and significantly improves TDOA positioning accuracy, especially under NLOS conditions. By integrating optimized TDOA technology with BDS/INS navigation, the proposed method enhances the reliability and precision of BDS in diverse application scenarios. It offers practical value in areas such as intelligent transportation, precision agriculture, and unmanned aerial vehicle navigation. The goal is to reduce the root mean square error (RMSE) of Ultra-Wideband (UWB)-based TDOA positioning to below 0.17 m under increased measurement noise, demonstrating a clear advantage over conventional methods through the proposed SSUKF-FA-RBF framework.

2 Related work

With the widespread application of GNSSs, particularly the growing significance of China's BDSs in precise positioning, achieving high accuracy in complex environments has become a key research challenge. The Kalman Filter (KF), as a widely used data fusion technique, plays a crucial role in enhancing positioning accuracy and system robustness in multi-sensor navigation systems [8]. For example, Chen et al. proposed a collaborative navigation framework based on a distributed adaptive EKF and model predictive control. Their approach significantly improved positioning accuracy, trajectory tracking, and error correction in the presence of multi-source noise and nonlinear dynamics, especially in dynamic and complex navigation scenarios [9]. Park demonstrated that the Adaptive Unscented Kalman Filter (AUKF) maintained robust performance during Global Positioning System (GPS) signal degradation or loss, yielding more accurate signal position estimates than conventional EKF and UKF methods [10]. Yin et al. developed an Error-State Kalman Filter (ESKF) combined with the Rauch-Tung-Striebel (RTS) smoothing algorithm, using data from inertial measurement units (IMU) and GNSS sensors. Their method improved positioning accuracy by approximately 3% in both linear and turning segments, compared to the EKF, demonstrating enhanced robustness and precision [11]. Similarly, Wu et al. introduced an adaptive iterative EKF integrating GNSS, INS, and UWB data, which produced stable and accurate estimates in complex coastal environments [12]. Yuan et al. proposed a robust KF algorithm based on singular value decomposition (SVD), achieving a 45.77% reduction in maximum error and a 4.7% decrease in RMSE compared to traditional KF-based information filtering approaches, thus improving overall positioning performance [13]. Neusypin et al. presented an INS/GPS correction method utilizing an improved adaptive nonlinear KF and a pre-flight error modeling strategy. By replacing conventional prior models with population data-driven error models, they addressed the limitations of traditional INS error handling. Flight tests confirmed the method's effectiveness in enhancing positioning accuracy [14].

While previous studies have achieved considerable advancements in integrating KF algorithms with BDSs, limitations remain. Traditional KF methods often underperform in complex environments-particularly in the presence of signal interruptions or severe multipath effects. Moreover, most existing approaches focus on fusing single-sensor data and lack comprehensive multi-source integration, which can limit system adaptability and robustness. To address these issues, the present study proposes an enhanced SSUKF algorithm that integrates the BDS and INS with a TDOA-based positioning strategy. Additionally, a RBF neural network optimized via the FA is introduced to improve convergence and accuracy. This combined framework aims to overcome the limitations of traditional KF methods, offering improved robustness and precision in dynamic and challenging environments.

The comparative results of mainstream filtering methods are summarized in Table 1.

Table 1: Comparative results of mainstream filtering methods

Author (Year)	Filter Type	Data Source	Best RMSE (m)	Computational Complexity	Key Innovation Highlights
Chen et al. (2025) [9]	DAEKF (Dual Adaptive Extended Kalman Filter) +DMPC (Distributed Model Predictive Control)	Cooperative Navigation/Robots	Lateral error: min 0.05 (straight path)	High	Adaptive noise covariance+ Model predictive control; multi-robot coordination
Yuan et al. (2024) [13]	SVD-KF (Kalman Filter)/ IF (Information Filter)	GNSS/INS/ Simulated	Max error reduced by 45.77%	Relatively High	Introduced SVD to dynamically adjust noise covariance
Park (2024) [10]	AUKF	GPS+ IMU/Vehicle	Not specified	Medium	Adaptive covariance handling under GPS outages; improved robustness

Neusypin et al. (2023) [14]	Adaptive NKF (Nonlinear Kalman Filtering)	INS/GPS/ Flight experiments	Not specified	Relatively High	Real INS error modeling pre-flight + GMDH (Group Method of Data Handling) group modeling
Wu et al. (2023) [12]	Adaptive Iterative Extended Kalman Filter (AIEKF)	GNSS+INS+UWB/ Outdoor	Not specified	Medium	Adaptive multi-sensor fusion
Yin et al. (2023) [11]	ESKF, ESKF-RTS	GNSS+IMU/ Tunnel tests	Lateral RMSE: min 0.206	High	Error-state modeling + RTS smoothing; 55.6%-70.8% RMSE improvement
The proposed model	SSUKF-FA-RBF	UWB TDOA/ Indoor	Best RMSE: 0.127	Moderate	Spherical Simplex Unscented Transformation (SSUT)-based sigma sampling + Firefly-optimized RBF; robust and precise under noise

As shown in Table 1, existing filtering algorithms exhibit distinct advantages in terms of accuracy or robustness. However, many depend on high computational resources or are designed for specific application scenarios, lacking a unified optimization framework suitable for nonlinear systems operating under high-noise conditions. In contrast, the proposed SSUKF-FA-RBF model combines an improved sigma-point sampling strategy with a neural network-based optimization approach. This hybrid framework delivers higher positioning accuracy than conventional filters while also achieving superior computational efficiency and generalization capability. These attributes make it especially well-suited for high-precision indoor positioning applications.

3 Research methodology

3.1 BDS

The BDS is a GNSS independently developed by China. Alongside the United States' GPS, Russia's GLONASS, and Europe's Galileo, BDS forms one of the four major global navigation systems. Its structural architecture is illustrated in Figure 1 [15].

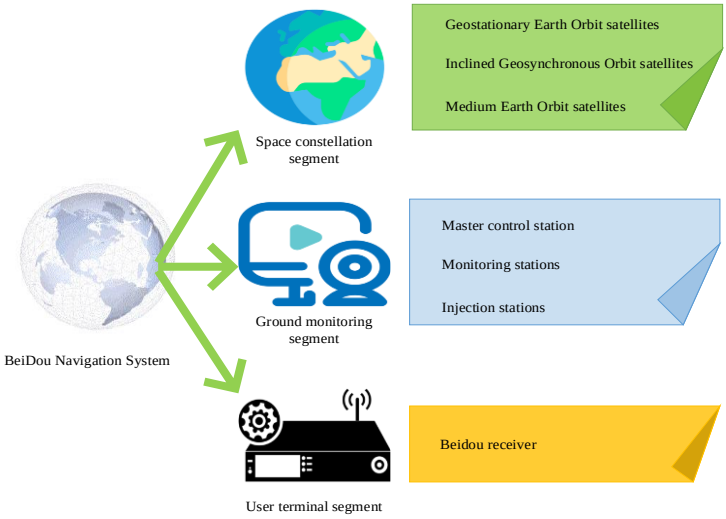

Figure 1: Hierarchical architecture and core components of the BDS

Figure 1 depicts the three-tiered architecture of BDS, comprising the space segment, ground segment, and user segment. The space segment includes satellites deployed in various orbital configurations that transmit multi-frequency signals to provide global coverage and high-precision positioning. The ground segment is responsible for satellite monitoring, data processing, and the dissemination of navigation data, ensuring the system's stability and reliability. The user segment encompasses a wide range of terminal devices that receive and process satellite signals to compute positioning information. This study leverages the BDS architecture by utilizing the multi-frequency signal transmission and extensive coverage of the space segment to enhance the nonlinear state estimation capabilities of the proposed SSUKF algorithm. Calibration data from the ground segment are employed to improve the reliability of observational inputs, contributing to greater filtering stability. At the user level, the integration of multi-source sensor data enables real-time data fusion within the SSUKF-FA-RBF

framework. Notably, the incorporation of TDOA-based auxiliary positioning in complex environments helps mitigate signal degradation, resulting in improved robustness and accuracy in positioning performance.

BDS provides dual- and multi-frequency signals, which enhance anti-interference performance and improve positioning accuracy. By incorporating high-precision positioning techniques such as Precise Point Positioning (PPP) and Real-Time Kinematic carrier phase positioning, BDS can achieve centimeter- to millimeter-level accuracy.

The integration of BDS with INS results in a multi-source navigation framework that combines the strengths of satellite and inertial navigation. INS estimates position using gyroscopes and accelerom, maintaining independence from external environmental influences but suffering from cumulative error over time. In contrast, the BDS offers globally precise positioning but is susceptible to signal degradation in obstructed environments, such as urban canyons and tunnels. Therefore, the BDS/INS integration leverages the complementary advantages of both systems, improving overall navigation robustness and accuracy [16].

BDS/INS integration commonly employs the KF for data fusion. The fundamental state and observation equations of the KF are as follows [17-20]:

$$\dot{X} = FX + GW \tag{1}$$

$$Z = HX + V \tag{2}$$

Here, X refers to the system state variable; F is the state transition matrix; G is the process noise matrix; W represents the process noise; Z stands for the observation quantity; H is the observation matrix; V denotes the observation noise.

The state prediction steps of KF are shown in Equations (2) and (3):

$$\hat{X}_{k|k-1} = F\hat{X}_{k-1|k-1} + GW \tag{3}$$

$$P_{k|k-1} = FP_{k-1|k-1}F^T + Q \tag{4}$$

The state update steps are given by follows:

$$K_k = P_{k|k-1}H^T(HP_{k|k-1}H^T + R)^{-1} \tag{5}$$

$$\hat{X}_{k|k} = \hat{X}_{k|k-1} + K_k(Z_k - H\hat{X}_{k|k-1}) \tag{6}$$

$$P_{k|k} = (I - K_kH)P_{k|k-1} \tag{7}$$

In these expressions, P represents the state covariance matrix; K denotes the Kalman gain; Q and R are the covariance matrices of the process and observation noise, respectively.

3.2 The improved SSUKF algorithm

Accurate positioning remains a fundamental challenge in mobile robotics, autonomous unmanned systems, and target tracking in complex and dynamic environments. The traditional EKF requires first-order Taylor expansion to nonlinear systems, which often introduces significant linearization errors and limits its effectiveness in handling highly nonlinear state estimation problems. In contrast, UKF employs unscented transformation to approximate the posterior distribution by propagating a set of carefully selected Sigma points through the nonlinear system dynamics. This method generally yields higher estimation accuracy than EKF, particularly in scenarios involving strong nonlinear and non-Gaussian noise. However, the symmetric sampling strategy of standard UKF may result in overly dispersed Sigma point distributions in high-dimensional state spaces. This dispersion increases the risk of cumulative filtering errors and degrades positioning accuracy over time [21, 22]. To address these limitations, this study adopts the SSUKF algorithm, which improves filtering performance by optimizing the distribution of Sigma points.

At the core of SSUKF is the SSUT, which replaces the symmetric sampling method of the conventional UKF with a spherical simplex sampling approach. This substitution effectively reduces the spread radius of Sigma points in high-dimensional spaces, mitigating error accumulation and enhancing numerical stability. Building on SSUT, SSUKF introduces several key improvements. First, it incorporates and systematically tunes the scaling factor α, the covariance weight adjustment parameter β, and the spread factor κ. These adjustments allow the Sigma-point distribution to more accurately reflect the system's nonlinear behavior, thereby improving both robustness and estimation precision. Second, SSUKF refines the calculation of mean and covariance weights by employing a corrected weighting formula. This correction results in a more balanced weight distribution and minimizes the bias errors commonly observed in standard UKF due to uneven weighting. Finally, the algorithm simplifies Sigma-point generation by replacing the computationally intensive Cholesky decomposition with SVD, thereby reducing computational redundancy. This structural optimization enhances processing efficiency without compromising estimation accuracy, making SSUKF particularly suitable for real-time, high-precision positioning applications.

If the mean of the system state variables is $\bar{x}$, then the selection of Sigma points for the improved SSUT strategy reads [23-27]:

$$\chi'_u = \begin{cases} \bar{x}, & i = 0 \\ \bar{x} + \alpha\sqrt{n+\kappa}S_i, & i = 1, \ldots, n \\ \bar{x} - \alpha\sqrt{n+\kappa}S_{i-n}, & i = n+1, \ldots, 2n \end{cases} \tag{8}$$

In Equation (8), S_i represents the i-th column of the covariance matrix S; α refers to the proportionality factor; κ is a hyperparameter; χ'_u denotes the i-th Sigma point; n refers to the dimension of the system state.

The weight assigned to each Sigma point consists of the mean weight W_i^m and the covariance weight W_i^c, computed as follows:

$$W_i^m = \begin{cases} \frac{W_0 - 1}{\alpha^2} + 1, & i = 0 \\ \frac{W_i}{\alpha^2}, & i \neq 0 \end{cases} \tag{9}$$

$$W_i^c = \begin{cases} W_0 + 1 - \alpha^2 + \beta, & i = 0 \\ \frac{W_i}{\alpha^2}, & i \neq 0 \end{cases} \tag{10}$$

Here, β a hyperparameter used to reduce approximation errors; W_i represents the initial weight of the i-th Sigma point; W_0 stands for the initial weight value.

The param α, β, and κ significantly influence the Sigma-point distribution and overall filtering accuracy within the SSUKF framework. The parameter α typically takes a small positive value (e.g., between 10^{-3} and 10^{-1}) to control the spread of the Sigma points. The parameter β adjusts the covariance weight's central tendency and is commonly set to 2 when the state distribution is Gaussian. The parameter κ acts as a secondary scaling factor stabilizing the term $n+\kappa$, where n is the state vector dimension; it is often set to 0 or $3-n$.

In this study, experimental tuning determined α=0.05, β=2, and κ=0 as optimal values, achieving a balance between estimation accuracy and numerical stability in high-precision positioning scenarios.

According to the selected Sigma points, the state variables undergo nonlinear transformation to calculate the predicted state mean and covariance. The expressions are as follows:

$$\hat{x}_{k+1} = \sum_{i=0}^{2n} W_i^m f(\chi'_{u,i}) \quad (11)$$

$$P_{k+1} = \sum_{i=0}^{2n} W_i^c [f(\chi'_{u,i}) - \hat{x}_{k+1}][f(\chi'_{u,i}) - \hat{x}_{k+1}]^T + Q \quad (12)$$

Here, $\hat{x}_{k+1}$ denotes the predicted mean state; $f(\chi'_{u,i})$ is the nonlinear state transition function applied to the i-th Sigma point; P_{k+1} represents the predicted covariance matrix; Q refers to the covariance matrix of process noise.

Using the predicted Sigma points, the observation mean and covariance are computed as:

$$\hat{z}_{k+1} = \sum_{i=0}^{2n} W_i^m h(\chi'_{u,i}) \quad (13)$$

$$P_{zz} = \sum_{i=0}^{2n} W_i^c [h(\chi'_{u,i}) - \hat{z}_{k+1}][h(\chi'_{u,i}) - \hat{z}_{k+1}]^T + R \quad (14)$$

P_{zz} represents the observed covariance matrix; $h(\chi'_{u,i})$ denotes the nonlinear observation function applied to the i-th Sigma point; R is the measurement noise covariance matrix; $\hat{z}_{k+1}$ refers to the predicted observation mean. The cross-covariance matrix P_{xz} between the states and observations is calculated by Equation (15):

$$P_{xz} = \sum_{i=0}^{2n} W_i^c [\chi'_{u,i} - \hat{x}_{k+1}][h(\chi'_{u,i}) - \hat{z}_{k+1}]^T \quad (15)$$

The Kalman gain is computed as Equation (16):

$$K = P_{xz} P_{zz}^{-1} \quad (16)$$

The updated state vector and covariance matrix are then given by follows:

$$x_{k+1} = \hat{x}_{k+1} + K(z_{k+1} - \hat{z}_{k+1}) \quad (17)$$

$$P_{k+1} = P_{k+1} - K P_{zz} K^T \quad (18)$$

In this context, K denotes the Kalman gain matrix; x_{k+1} refers to the updated state estimate; z_{k+1} is the actual observation; P_{k+1} represents the updated covariance matrix of the state.

Figure 2 presents the complete process of the proposed integrated navigation algorithm based on the improved SSUKF.

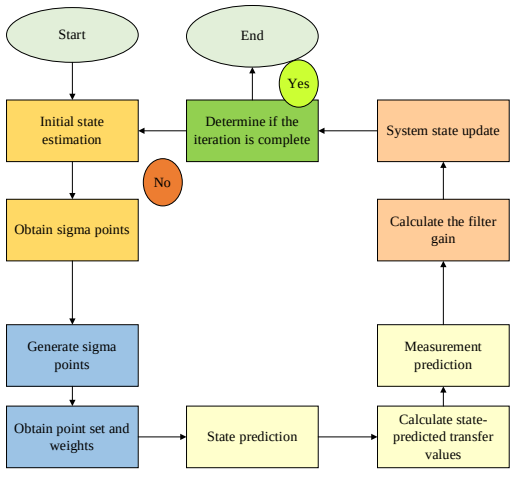

(a) The combined navigation process under the improved algorithm

```
1:  Initialize dimensions:
      n = dimension of state vector x
      lambda = alpha^2 * (n + kappa) - n

2:  Compute sigma point weights:
      Wm[0] = lambda / (n + lambda)
      Wc[0] = Wm[0] + (1 - alpha^2 + beta)
      for i = 1 to 2n:
        Wm[i] = 1 / [2 * (n + lambda)]
        Wc[i] = Wm[i]

3:  Generate sigma points:
      S = Cholesky decomposition of (n + lambda) * P
      sigma_points[0] = x
      for i = 1 to n:
        sigma_points[i]     = x + column_i(S)
        sigma_points[i + n] = x - column_i(S)

4:  Predict sigma points through transition function:
      for i = 0 to 2n:
        sigma_points_pred[i] = f(sigma_points[i])

5:  Compute predicted state mean:
      x_pred = sum over i: Wm[i] * sigma_points_pred[i]
```

```
6:  Compute predicted covariance:
      P_pred = sum over i: Wc[i] * (sigma_points_pred[i] -
x_pred)^2 + Q

7:  Predict sigma points through observation function:
      for i = 0 to 2n:
        z_sigma[i] = h(sigma_points_pred[i])

8:  Compute predicted observation mean:
      z_pred = sum over i: Wm[i] * z_sigma[i]

9:  Compute innovation covariance:
      P_zz = sum over i: Wc[i] * (z_sigma[i] - z_pred)^2 + R

10: Compute cross covariance:
      P_xz = sum over i: Wc[i] * (sigma_points_pred[i] -
x_pred) * (z_sigma[i] - z_pred)^T

11: Compute Kalman gain:
      K = P_xz * inverse(P_zz)

12: Update state estimate:
      x = x_pred + K * (z_actual - z_pred)

13: Update covariance:
      P = P_pred - K * P_zz * K^T
```

(b) SSUKF-based state estimation code

Figure 2: Combined navigation flow with improved algorithm and SSUKF-based state estimation code

The process begins with an initial state estimation and dynamically selects either the state update path or the Sigma-point generation path according to a set of adaptive iteration termination criteria. The spherical simplex sampling strategy optimizes the Sigma-point distribution, effectively reduces redundant sampling, and improves computational efficiency. Concurrently, the refined weighting mechanism enhances the stability and accuracy of nonlinear state estimation.

The contributions of this study are reflected in three key aspects. First, the flowchart explicitly illustrates the closed-loop feedback structure and core computational steps of SSUKF, thereby clarifying how the algorithm mitigates linearization errors in high-dimensional spaces. Second, the introduction of a dynamic iteration termination mechanism reduces unnecessary computations and significantly accelerates algorithm execution, demonstrating the effectiveness of the performance optimization. Third, the annotated mathematical formulations within the process provide a clear and reproducible framework that supports future algorithmic enhancements and comparative research.

In each filtering cycle, the standard UKF generates $2n$+1 symmetric Sigma points, with the main computational burden arising from the Cholesky decomposition of the covariance matrix and two rounds

of nonlinear transformation. The corresponding time complexity typically ranges from $O(n2)$ to $O(n3)$. In contrast, SSUKF also utilizes $2n$+1 Sigma points but constructs them using spherical simplex sampling based on SVD or a simplified orthogonal vector computation method. This approach eliminates redundant symmetric configurations, yielding a more compact Sigma-point distribution and contributing to enhanced numerical stability. Additionally, the inclusion of tunable param α, β, and κ in the weight and covariance computation further improves estimation precision. This adjustment enables SSUKF to maintain a comparable computational complexity to the standard UKF while achieving superior performance, particularly in high-dimensional nonlinear systems. When the system dimension n is relatively small, SSUKF maintains time complexity similar to UKF but significantly outperforms it in terms of filtering accuracy and numerical robustness.

In summary, the improved SSUKF algorithm surpasses the standard UKF in structural design, Sigma-point selection strategy, and overall numerical stability. It retains the computational efficiency of the original framework while delivering enhanced estimation accuracy and resilience to noise, making it particularly well-suited for high-dynamic and high-dimensional integrated navigation scenarios.

3.3 Optimization of the TDOA method

TDOA is a widely adopted localization technique that estimates the position of a signal source by analyzing the time differences of signal arrivals at multiple spatially distributed receivers. While effective in theory, the practical accuracy of TDOA is often compromised by signal propagation conditions, receiver geometry, and measurement noise. In particular, NLOS environments introduce substantial errors in TDOA measurements, significantly degrading localization performance [28].

To address these challenges and enhance positioning accuracy, this study introduces a RBF neural network to optimize the extraction and utilization of time difference features. The RBF neural network's structure under TDOA is displayed in Figure 3 [29].

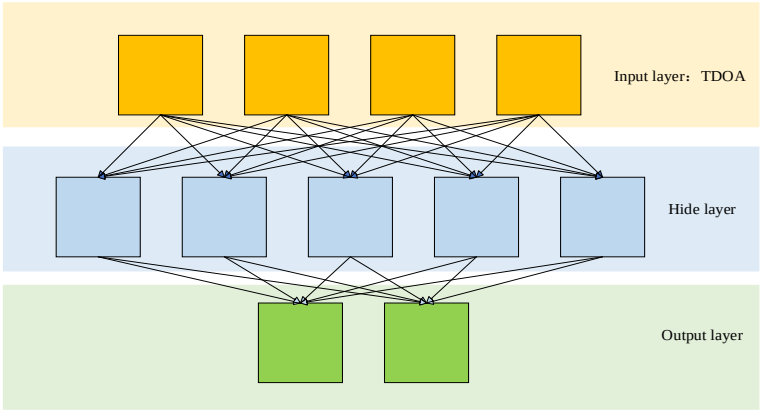

Figure 3: Architecture of the radial basis function neural network for TDOA-based localization

As illustrated in Figure 3, the proposed model adopts a standard three-layer RBF neural network structure, comprising an input layer, a hidden layer with radial basis neurons, and an output layer. This architecture is characterized by strong nonlinear mapping capabilities and robust generalization, making it particularly suitable for positioning tasks. The input layer accepts feature vectors derived from TDOA measurements. The hidden layer applies a nonlinear transformation using Gaussian kernel functions, effectively capturing the spatial distribution characteristics of the input data. The output layer is responsible for regressing the final position coordinates (x,y,z). The three-layer RBF network is theoretically capable of approximating any continuous function, offering both simplicity in design and high training efficiency. These properties make it especially suitable for TDOA scenarios, where the input dimensionality is relatively low and the relationship between input features and output coordinates exhibits significant nonlinearity. Compared to deeper multi-layer networks, the RBF neural network achieves a favorable trade-off between modeling capacity and computational cost, rendering it ideal for small-scale, high-precision positioning applications.

The hierarchical structure of the proposed TDOA-RBF model clearly visualizes the process by which time difference features are transformed into spatial coordinates through nonlinear mapping. This foundation enables the application of the FA to optimize the RBF network param, including the centers and widths of the Gaussian kernel functions. The use of adjustable-width kernels enhances the model's resilience to noise, a crucial advantage in high-interference environments. Experimental results demonstrate that the integration of the FA with RBF training significantly improves localization performance. In particular, the SSUKF-FA-RBF model achieves a RMSE as low as 0.127 m under high-noise conditions. This hybrid approach also mitigates the limitations of conventional Gradient Descent (GD) methods, which are often prone to local optima, by leveraging the global search capabilities of the FA. As such, the proposed method offers a novel and efficient solution to the TDOA localization problem, delivering both high accuracy and low computational complexity.

The input feature vector in the TDOA method

consists of time difference measurements between a signal source and multiple receivers. In practical data acquisition, this vector is affected by several noise sources, including Gaussian measurement errors, receiver clock biases, and NLOS multipath interference. To improve data quality and meet neural network training requirements, this study applies a series of preprocessing steps to the TDOA feature vectors before network input. First, mean normalization eliminates dimensional discrepancies among different features. Second, outlier filtering uses the z-score method to remove data points deviating by more than three standard deviations from the mean. Third, Gaussian white noise modeling assumes TDOA errors follow a zero-mean Gaussian distribution with adjustable variance to simulate realistic ranging errors and enhance model robustness to environmental disturbances. These preprocessing steps improve numerical stability and better reflect the perturbation characteristics of complex signal propagation environments, contributing to more reliable learning performance within the RBF neural network framework.

The output of the RBF neural network is formally described by Equations (19) and (20) [30, 31]:

$$y = \sum_{i=1}^{N} w_i \cdot \phi(\| x - c_i \|) \tag{19}$$

$$\phi(\| x - c_i \|) = e^{-\frac{(x-c_i)^2}{2\sigma^2}} \tag{20}$$

In these equations, y the network output vector corresponding to the estimated position; N denotes the number of hidden layer neurons; $\phi(\| x - c_i \|)$, w_i, and c_i represent the activation function, weight, and center of the i-th node; x means the input vector; σ stands for the width parameter.

Following the initial RBF-based position estimation, a post-processing refinement step is applied to further enhance localization accuracy. A commonly used method in this context is the least squares optimization, which minimizes the total squared error between the estimated and actual measurements. The optimization objective is formulated as Equation (21):

$$\min_{x} \sum_{i=1}^{M} \| f(x) - y_i \|^2 \tag{21}$$

In Equation (21), x denotes the position of the signal source to be optimized; $f(x)$ stands for the predicted position derived from the TDOA model; y_i represents the actual measured position; M refers to the number of measurement samples.

The RBF neural network achieves precise positioning prediction by learning the relationship between input features and actual locations. The network's optimization involves adjusting weights and bias param using the FA to avoid local optima and accelerate the convergence process. The specific steps are as follows. First, a population of "firefly" individuals is initialized, with each individual representing a potential solution, i.e., a combination of RBF network param, including centers, widths, and output weights. Next, the performance of each firefly is evaluated by calculating its fitness value, usually determined by the prediction error of the RBF network. A smaller error corresponds to a higher fitness value, indicating better performance. Then, based on fitness, FA updates the positions of individuals by simulating the light attraction behavior of fireflies in nature. Fireflies are attracted to others based on brightness, enabling local search within the solution space, where brightness is proportional to solution quality. Through iterative updates, the firefly population gradually converges toward the optimal solution. During each iteration, firefly movement considers brightness differences and introduces random perturbation to avoid getting trapped in local optima. Lastly, after multiple iterations, FA identifies the optimal RBF network param that minimize the network's error, thus enhancing its performance in data prediction and classification tasks. The workflow of the FA-RBF model is illustrated in Figure 4.

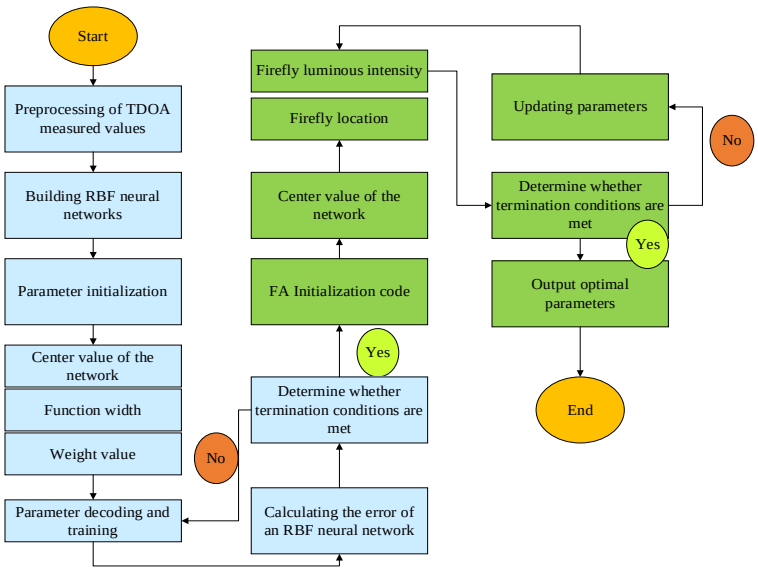

Figure 4: The process of the FA-RBF model

To further enhance the system's nonlinear modeling capability, an RBF neural network module is introduced

based on the Kalman filter output. Specifically, the current state estimates from the filter (such as position $\hat{x}$ and velocity $\hat{v}$) are combined with the original TDOA observation residuals-the differences between measured values and filter predictions-to form the input vector for the RBF network. The RBF network learns the nonlinear mapping of these errors and models the prediction residuals through radial basis kernel functions to perform compensation. During training, the network param are optimized via backpropagation or the FA to minimize prediction errors. In the inference phase, the RBF network can correct nonlinear errors in the Kalman filter's predictions in real time, thereby improving the accuracy and robustness of the final positioning output. The RBF output serves as a reference for the next filtering cycle's prediction, creating a semi-closed loop iterative optimization structure that strengthens the system's dynamic adjustment capability. This design demonstrates effective error control and convergence performance in experimental evaluations.

In complex dynamic environments, such as urban canyons, under elevated bridges, with building obstructions, or during high-speed motion, the measurement noise encountered by navigation receivers often exhibits instability, sudden bursts, and nonlinear variations. To address these challenges, the proposed SSUKF-FA-RBF hybrid framework possesses strong dynamic noise adaptation features in its structural design. First, during the Kalman filtering stage, both the process noise covariance matrix and the observation noise covariance matrix are dynamically updated based on the sensor's current environmental conditions, allowing flexible response to varying noise levels. Second, the RBF neural network uses the TDOA measurement residuals as core inputs to learn the nonlinear relationship between residuals and true errors, enabling real-time modeling and correction of non-stationary noise characteristics during operation. Additionally, the FA adaptively optimizes the RBF network's centers, widths, and weights, ensuring strong convergence and generalization performance even under diverse noise disturbances.

4 Experimental design and performance evaluation

4.1 Dataset collection and experimental setting

The data utilized in this study are derived from the Smart Positioning and Navigation Technology-Position Orientation System (SmartPNT-POS) dataset and the UWB TDOA dataset. The SmartPNT-POS dataset comprises extensive observations from vehicle-mounted, airborne, and shipborne platforms, totaling 30 sets of data. It includes GNSS reference values, rover observations, precise products for PPP computation, IMU data, and reference solutions obtained through post-processing using Inertial Explorer. The IMU data are stored in .imr format and extracted using the provided "ReadIMR.cpp" program, adopting the right-front-up coordinate system consistent with the IMU orientation. The reference attitude solutions from IE are also based on the right-front-up coordinate system relative to the carrier frame. Vehicle-mounted data lack lever-arm information from the IMU to the rear axle; however, the baseline lengths labeled "X-LL," "Y-LL," and "Z-LL" in the reference solutions correspond to the East-North-Up coordinate system with the reference station as the origin. This dataset offers high-quality, diverse real-world measurements, making it well suited for research and development in GNSS/INS integrated navigation algorithms. The UWB TDOA dataset provides UWB time-difference-of-arrival measurements obtained from the Bitcraze Loco positioning system. It contains collected TDOA measurements synchronized with ground-truth data from the Vicon motion capture system. The training data involve seven distinct UWB anchor constellations, which are used to correct TDOA measurement biases and improve state estimation accuracy. The dataset is processed using Python tools and includes spatial coordinates (x, y, z), UWB TDOA measurements, timestamps, and other relevant information, making it suitable for high-precision indoor positioning, robotic navigation, and logistics tracking research. The experiments in this study are divided into two parts: (1) performance validation of BDS/INS integrated navigation using the publicly available SmartPNT-POS dataset, which encompasses BDS observations and INS data across multiple scenarios; (2) optimization experiments of the TDOA method based on the UWB TDOA dataset. These two datasets are independently collected and distinctly purposed, ensuring targeted and reliable algorithm evaluation.

The UWB TDOA dataset is collected using the Bitcraze Loco positioning system, while the ground truth reference values are provided by the high-precision Vicon motion capture system. Both systems are precisely synchronized using absolute timestamps measured in milliseconds. Due to the different sampling rates of the two systems-100 Hz for the Vicon system and 80 Hz for the UWB system-the TDOA data are linearly interpolated to 100 Hz. This ensures full temporal alignment with the Vicon data, allowing each TDOA record to be matched with an accurate real-world position label. To improve data quality and enhance the effectiveness of model training, several preprocessing procedures are applied. First, abnormal jump values and duplicate timestamp entries are removed to eliminate inconsistencies. Second, linear interpolation is used to fill in occasional missing observations, preserving the continuity of the time series. Third, all input features, including TDOA residuals and time variables, are normalized to have zero mean. This step eliminates scale differences and promotes faster convergence during network training. Finally, the dataset is divided into training, validation, and test sets in fixed proportions. To ensure independent evaluation and robust generalization, care is taken to exclude any overlapping trajectories between the training and test sets. These preprocessing steps significantly improve the accuracy and consistency of the dataset, thereby establishing a

reliable foundation for validating the performance of the proposed algorithm.

This study conducts experiments in a Windows 10 operating system environment using Matrix Laboratory Release (R) 2021b. A UWB channel model is established under NLOS conditions. The neural network adopts a three-layer architecture comprising seven input nodes, ten hidden layer neurons, and two output nodes. The number of neurons in the hidden layer is fixed at 10. During training, the batch size is initially set to 8, and additional experiments are conducted using batch sizes of 4, 8, 16, and 32 to evaluate the impact of batch size on training performance. The FA is employed to optimize the neural network param. The algorithm configuration includes a light intensity attenuation rate of 1, a population size of 30, a decay factor of 0.1, a minimum attractiveness coefficient of 0.2, and a maximum attractiveness coefficient of 2. The maximum number of iterations for all models is set to 100.

Although this study uses the UWB TDOA dataset for modeling and validation-providing robust experimental support for typical high-precision indoor positioning scenarios-it further examines the generalizability of the proposed method to explore its broader applicability. From a feature structure perspective, the SSUKF-FA-RBF model takes time-difference feature vectors as input, indicating a degree of independence from specific signal types. This design suggests that the model has the potential to be transferred to other ranging modalities. Although different sensors may exhibit variations in error characteristics, sampling frequencies, and propagation models, the proposed method can be extended to non-UWB sensor systems or outdoor environments through appropriate input normalization and noise model adaptation. Additionally, the robust design of the filtering component enhances the model's capacity to cope with environmental complexity, supporting its scalability.

To ensure objectivity and generalizability in performance evaluation, this study adopts a standardized dataset partitioning approach. The original data are segmented sequentially by timestamp into 70% for training, 15% for validation, and 15% for testing. The training set is used to learn the param of the RBF neural network, the validation set is employed for tuning hyperparam and preventing overfitting, and the test set is reserved for final performance evaluation and generalization verification. All data splits maintain consistent spatial distributions within each subset, preserving representative anchor point configurations and signal characteristics, thereby enhancing the reproducibility and realism of the experimental results.

To establish a unified framework suitable for high-precision indoor positioning, this study proposes the SSUKF-FA-RBF model, which integrates two core technical components across distinct stages. The first component is a SSUKF based on a BDS/INS fusion architecture. The second component is a machine learning optimization approach (FA-RBF) that combines TDOA measurement features with a Radial Basis Function neural network. The SSUKF module enhances the prediction accuracy of the BDS/INS system under nonlinear and high-noise conditions by incorporating a hyperspherical simplex sampling mechanism (Figure 5). The SSUKF-FA-RBF module extends this approach to TDOA-based positioning by employing SSUKF for dynamic state prediction and using the RBF network to perform nonlinear compensation for TDOA errors, thereby improving the final position estimation (Figure 6).

Although Figures 5 and 6 present two distinct sets of experimental results, they correspond to different processing stages within the same system framework. Figure 5 evaluates the estimation accuracy of the standalone SSUKF within a conventional BDS/INS integrated navigation system, highlighting the performance improvements resulting from the enhanced filter structure. In contrast, Figure 6 assesses the integrated SSUKF and FA-RBF scheme under TDOA constraints, demonstrating its generalization capability in practical communication-based ranging systems. In this context, the SSUKF functions both as the core filtering mechanism in the BDS/INS system and as the dynamic state predictor in the TDOA-RBF module. These two components-state estimation and error compensation-operate sequentially and synergistically, forming a unified high-precision positioning architecture capable of fusing multi-source navigation data. This structural design enables coherent and functionally consistent integration of the SSUKF and TDOA-RBF systems, ensuring logical alignment across system modeling, filtering architecture, and error correction strategies.

4.2 Performance evaluation

This study compares the positioning error of the proposed algorithm in integrated navigation against the Incremental Extended Kalman Filter (IEKF), Covariance Kalman Filter (CKF), Extended Kalman Filter (EKF), UKF, and the SSUT algorithms. The selected Kalman filter variant and the RBF neural network operate not independently but as a cascaded hybrid positioning system. In this structure, the Kalman filter predicts and updates the target state variables, such as position and velocity. Its outputs serve both as intermediate navigation estimates and as inputs to the subsequent neural network module. This design fully leverages the Kalman filter's strengths in temporal modeling and dynamic system prediction while utilizing the neural network to address nonlinear errors and complex TDOA measurement residuals, thereby improving overall positioning accuracy in complex environments. The specific results are depicted in Figure 5.

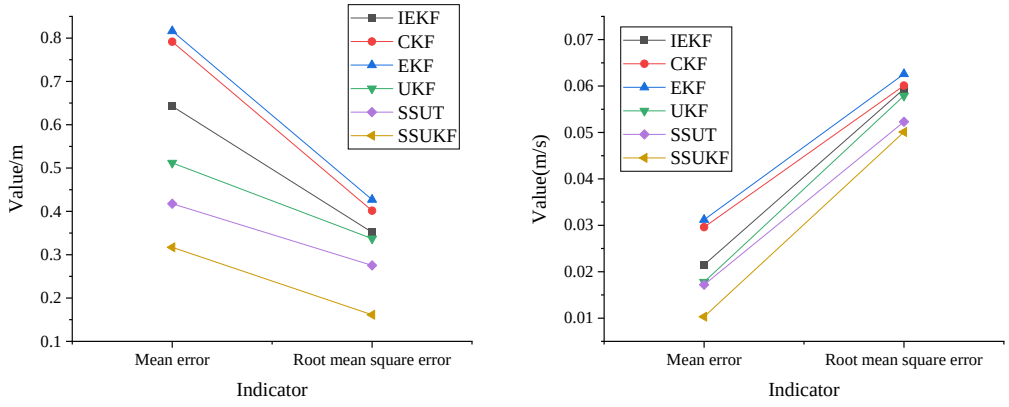

(a) Position positioning error (b) Speed positioning error

Figure 5: Comparison results of positioning errors in integrated navigation under different algorithms

Analysis of Figure 5a indicates that the SSUKF algorithm demonstrates a significant advantage in reducing positioning error. Specifically, the mean position error of SSUKF is 0.3172 m (m), substantially lower than IEKF (0.6426 m), CKF (0.7916 m), and EKF (0.8163 m). This highlights the effectiveness of SSUKF in improving positioning accuracy. Regarding RMSE in position estimation, SSUKF achieves 0.1614 m, markedly lower than IEKF (0.3518 m), CKF (0.4015 m), EKF (0.4271 m), and UKF (0.3371 m). These results demonstrate that SSUKF effectively reduces error fluctuations and enhances overall positioning accuracy. Collectively, they confirm the superiority of SSUKF in improving precision, reducing computational burden, and enhancing system stability.

Figure 5b further shows that SSUKF outperforms traditional algorithms in velocity positioning accuracy. The mean velocity error of SSUKF is 0.0103 m per second (m/s), significantly lower than IEKF (0.0215 m/s), CKF (0.0296 m/s), EKF (0.0312 m/s), and UKF (0.0178 m/s). This improvement is attributed to the optimized Sigma point sampling strategy, which effectively reduces velocity positioning errors. In terms of velocity RMSE, SSUKF achieves 0.0501 m/s, outperforming IEKF (0.0594 m/s), CKF (0.0601 m/s), EKF (0.0626 m/s), and UKF (0.0579 m/s). Compared to these methods, SSUKF exhibits lower error fluctuation, thereby enhancing velocity positioning stability and reliability. These results collectively demonstrate that SSUKF delivers superior performance in real-world applications, especially in high-precision positioning scenarios where it clearly surpasses traditional methods.

The computation time results of various algorithms in integrated navigation are presented in Table 2.

Table 2: Calculational time of various algorithms in integrated navigation

Algorithm	Computation Time(Mean±Standard Deviation)	95% Confidence Interval
IEKF	13.50±0.27	[13.32,13.68]
CKF	14.10±0.32	[13.88,14.32]
EKF	15.20±0.25	[15.03,15.37]
UKF	12.80±0.30	[12.59,13.01]
SSUT	7.73±0.12	[7.65,7.81]
SSUKF	7.69±0.10	[7.61,7.77]

Analysis of Table 2 reveals significant differences in computational efficiency among the Kalman filter algorithms applied to integrated navigation tasks. Traditional algorithms such as the EKF (15.20 ± 0.25 seconds) and CKF (14.10 ± 0.32 seconds) require relatively longer computation times, while the UKF (12.80 ± 0.30 seconds) performs better. In contrast, the SSUT (7.73 ± 0.12 seconds) and the SSUKF (7.69 ± 0.10 seconds) achieve the shortest computation times and demonstrate smaller fluctuations and tighter confidence intervals, indicating superior stability across multiple runs. The SSUKF significantly reduces computational cost while maintaining high accuracy, making it particularly suitable for real-time demanding applications such as indoor navigation and robotic positioning. Experimental results confirm its dual advantages in both time efficiency and robustness.

The comparison of positioning recognition performance of different models under the TDOA method is illustrated in Figure 6.

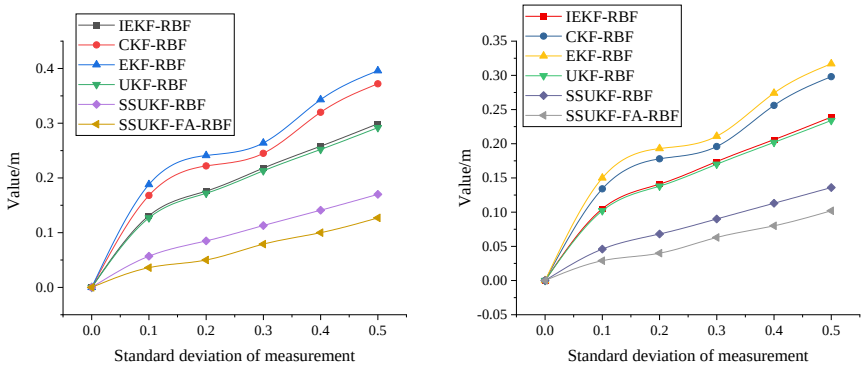

Figure 6: Comparison results of positioning recognition performance of various models under the TDOA method

Analysis of Figures 6a and 6b reveals that the SSUKF-RBF model demonstrates excellent RMSE performance, with RMSE values increasing from 0.057 m (standard deviation 0.1 m) to 0.17 m (standard deviation 0.5 m). This model achieves the highest accuracy under all tested conditions, indicating strong robustness and the ability to maintain low error levels across varying environments. The SSUKF-FA-RBF model achieves the lowest RMSE values across all noise levels, increasing from 0.036 m (standard deviation 0.1 m) to 0.127 m (standard deviation 0.5 m). Its relatively slow error growth rate and sustained low RMSE under high noise demonstrate its advantages in positioning accuracy and robustness. Overall, the SSUKF-FA-RBF model attains the best positioning accuracy across all test conditions, particularly excelling at low measurement standard deviations, where its RMSE is significantly lower than that of competing algorithms. As measurement standard deviation increases, the mean absolute errors (MAE) of all models rise, reflecting greater positioning errors. Among these, IEKF-RBF, CKF-RBF, EKF-RBF, and UKF-RBF exhibit relatively higher MAE values. At a measurement standard deviation of 0.5, EKF-RBF's MAE reaches 0.317 m, and UKF-RBF's is 0.234 m. In contrast, the improved SSUKF-RBF and SSUKF-FA-RBF models maintain substantially lower MAE values of 0.136 m and 0.102 m, respectively, demonstrating superior positioning accuracy and stronger resistance to noise. Notably, the SSUKF-FA-RBF model exhibits excellent robustness and stability across both low- and high-error conditions, underscoring its superior performance in TDOA-based positioning applications.

To further assess the adaptability of each model under varying environmental conditions and identify potential failure scenarios, this study conducts an in-depth analysis of error variation trends observed in the comparative experimental data. The SSUKF-FA-RBF model consistently maintains the lowest RMSE and MAE across all measurement noise levels, with standard deviations ranging from 0.1 m to 0.5 m, demonstrating strong noise resilience and stability. This model performs particularly well in NLOS simulated environments; as measurement noise increases, its error growth rate remains significantly lower than that of other models, indicating superior robustness amid multipath effects and signal occlusion. In contrast, traditional algorithms such as EKF-RBF, CKF-RBF, and IEKF-RBF experience considerable accuracy degradation under high-noise NLOS conditions or in complex urban areas. When the measurement standard deviation reaches 0.5 m, EKF-RBF's RMSE rises to 0.396 m and MAE to 0.317 m, with errors doubling and fluctuations intensifying. This reveals clear limitations in handling highly nonlinear or uncertain scenarios. UKF-RBF retains some accuracy advantages in urban or partially obstructed environments; however, as measurement noise increases beyond 0.3 m, its error escalates rapidly, suggesting that the Sigma point strategy may lack stability under high-dimensional disturbances. From a computational efficiency perspective, although the SSUKF-FA-RBF model achieves the highest accuracy, its network training and optimization require additional computational resources. Therefore, it is most suitable for applications prioritizing precision and high-value outcomes. Conversely, the SSUKF core offers a favorable balance between accuracy and computation time (7.69 ± 0.10 seconds), making it especially appropriate for deployment in resource-constrained indoor robotic systems or edge computing devices, where real-time performance and deployment flexibility are critical. In summary, the SSUKF-FA-RBF model is well-suited for complex, dynamic, or interference-prone high-precision positioning tasks, whereas the SSUKF alone is preferable for indoor navigation applications with strict real-time requirements. Traditional filtering algorithms remain appropriate for environments characterized by low noise levels and stable sensor channels. The error analysis and adaptability comparison under varying noise conditions validate the proposed method's advantages and robustness across diverse positioning scenarios.

To enhance the statistical rigor of this study's results, a repeated trial mechanism and statistical inference methods were incorporated based on the original experiments. Specifically, each filtering algorithm underwent ten independent repeated trials under identical test conditions. Position and velocity errors were reported as mean ± standard deviation to capture the variability and stability of model performance. Furthermore, to

account for potential randomness influencing differences in error outcomes across algorithms, paired sample t-tests were conducted to assess the statistical significance of differences in error metrics between the proposed SSUKF and other mainstream algorithms, including EKF, UKF, and SSUT. The detailed findings are summarized in Tables 3 and 4.

Table 3: Comparison of positional positioning errors

Indicator	IEKF	CKF	EKF	UKF	SSUT	SSUKF
Mean error (m)	0.6426±0.0213	0.7916±0.0241	0.8163±0.0205	0.5119±0.0182	0.4176±0.0158	0.3172±0.0124
RMSE (m)	0.3518±0.0115	0.4015±0.0126	0.4271±0.0133	0.3371±0.0109	0.2754±0.0091	0.1614±0.0083
P-value (SSUKF)	0.0003	0.0001	0	0.0012	0.0047	--
Significance	Yes	Yes	Yes	Yes	Yes	--

Table 4: Speed positioning error comparison

Indicator	IEKF	CKF	EKF	UKF	SSUT	SSUKF
Mean error (m/s)	0.0215±0.0021	0.0296±0.0017	0.0312±0.0018	0.0178±0.0013	0.0172±0.0010	0.0103±0.0008
RMSE (m/s)	0.0594±0.0032	0.0601±0.0036	0.0626±0.0030	0.0579±0.0024	0.0523±0.0020	0.0501±0.0015
P-value (SSUKF)	0.0009	0.0005	0.0002	0.0151	0.0376	--
Significance	Yes	Yes	Yes	Yes	Yes	--

Tables 3 and 4 present the average errors and RMSEs for position and velocity estimation tasks, respectively. Table 3 shows that the SSUKF algorithm achieves the best position estimation performance, with an average error of 0.3172 ± 0.0124 m and an RMSE of 0.1614 ± 0.0083 m. This performance significantly exceeds that of traditional EKF (RMSE of 0.4271 ± 0.0133 m) and UKF (RMSE of 0.3371 ± 0.0109 m). Notably, SSUKF's RMSE is approximately 24% lower than that of the second-best algorithm, SSUT, demonstrating that optimizing the sigma point distribution through spherical simplex transformation effectively enhances filter accuracy in highly nonlinear environments. Additionally, SSUKF exhibits smaller error standard deviations, indicating more stable and robust positioning. The paired t-test results confirm that differences in position error between SSUKF and all other algorithms are statistically significant ($p < 0.01$), reinforcing the scientific validity of the observed accuracy improvements.

Table 4 illustrates that SSUKF also leads in velocity estimation accuracy, achieving an average error of 0.0103 ± 0.0008 m per second and an RMSE of 0.0501 ± 0.0015 m per second. This significantly outperforms UKF (RMSE of 0.0579 ± 0.0024 m/s) and EKF (RMSE of 0.0626 ± 0.0030 m/s). These results confirm that SSUKF not only improves position estimation but also delivers superior accuracy and stability in dynamic velocity estimation. Among the alternatives, IEKF performs slightly better in velocity error than CKF and EKF but remains inferior to SSUKF. Paired t-tests indicate that velocity error differences between SSUKF and other algorithms are statistically significant ($p < 0.05$), further substantiating the effectiveness of the proposed approach.

In summary, the comparative analysis of position and velocity errors demonstrates that SSUKF, through its enhanced sigma point sampling and weighting design, significantly improves filter adaptability to nonlinear, high-noise systems, yielding dual enhancements in positioning accuracy and dynamic estimation. The reductions in mean error and standard deviation not only reflect improved measurement precision but also confirm the approach's stability and reliability, fulfilling the stringent demands of real-time navigation systems. The validation of statistical significance provides strong evidence for the scientific soundness of the proposed method and robustly supports the study's conclusions.

During the neural network training process, batch size significantly influences the model's learning efficiency and stability. Accordingly, this study conducted comparative experiments using four typical batch sizes: 4, 8, 16, and 32. Each batch size configuration was tested with 10 repeated experiments, and the results were reported as mean ± standard deviation to ensure robustness and statistical reliability. The detailed error performances are summarized in Table 5.

Table 5: Comparison of localization error under different batch sizes

Batch Size	Positioning Error (Mean±Standard Deviation)	Velocity Error (Mean±Standard Deviation)
4	0.185±0.012m	0.053±0.004m/s
8	0.161±0.008m	0.050±0.002m/s
16	0.172±0.010m	0.052±0.003m/s
32	0.180±0.013m	0.054±0.005m/s

The results in Table 5 reveal that smaller batch sizes, such as 4, promote faster model convergence but cause greater error fluctuations. In contrast, larger batch sizes, such as 32, produce smoother training processes but substantially increase training time. When the batch size is set to 8, the model attains the best average performance in both position and velocity errors, accompanied by relatively low variance. This outcome demonstrates a well-balanced trade-off between training stability and generalization capability. Therefore, a batch size of 8 is selected as the primary experimental configuration, optimizing training stability, computational efficiency, and prediction accuracy.

To validate the effectiveness of the proposed FA-RBF optimization strategy, this study conducted comparative experiments with two widely used optimization methods: standard GD and Particle Swarm Optimization (PSO). The experimental results are presented in Figure 7.

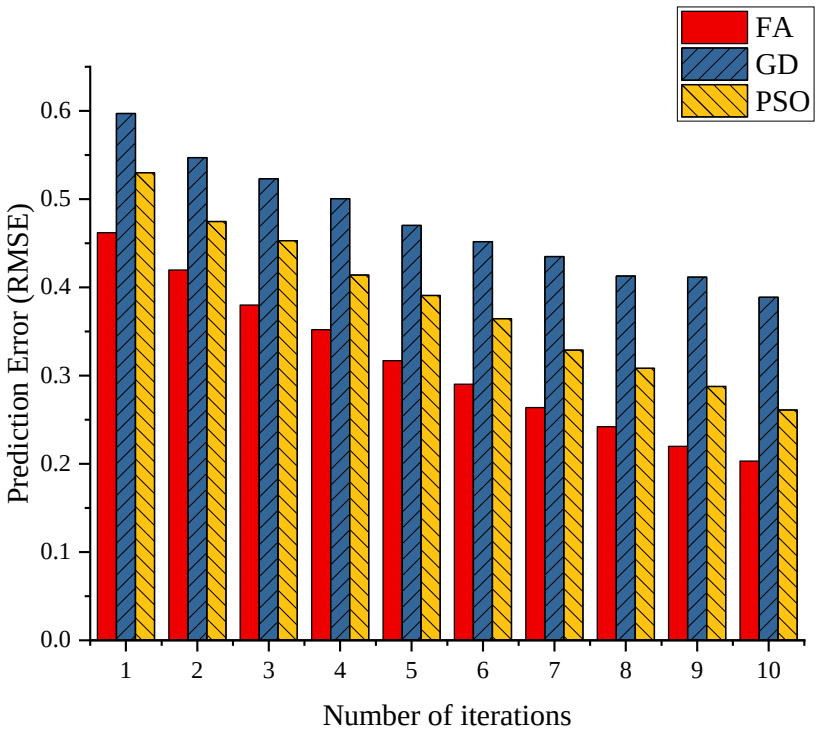

Figure 7: Comparison of optimization errors in TDOA-RBF models

As illustrated in Figure 7, under identical initial conditions and iteration counts, the RBF network optimized by the FA achieves lower prediction errors and faster convergence in the TDOA positioning task. Unlike GD, the FA does not rely on gradient information, thereby avoiding the common issue of becoming trapped in local optima within non-convex loss landscapes. Compared to PSO, the FA employs a brightness-based attraction mechanism that enables more effective global exploration and stable convergence. Additionally, the stochastic perturbation mechanism incorporated into the FA enhances its ability to escape local extrema in complex search spaces. Overall, the evaluation results demonstrate that the FA-RBF optimization strategy provides a favorable balance between error minimization and convergence efficiency, making it particularly well-suited for optimizing TDOA positioning models in complex and highly nonlinear scenarios.

The performance advantages and applicable scenarios of the evaluated models across typical environments-including NLOS, urban, and indoor conditions-are summarized in Table 6.

Table 6: Comparison of algorithm applicability in different positioning environments

Algorithm	Indoor (Line of Sight) Performance	Urban Semi-Obstructed	NLOS / High-Noise	Typical Failure Scenario	Recommended Use Cases
IEKF-RBF	Fair, unstable accuracy	Poor, high error rise	Poor, prone to divergence	Multipath interference; strong nonlinearity	Open environments with low noise
CKF-RBF	Moderate, stable	Poor, slow convergence	Weak, significant degradation	High-dimensional noise; discontinuous observations	Structured environments with high-precision sensors
EKF-RBF	Acceptable, average	Weak, sensitive to obstruction	Poor, accumulative error	Linearization bias; delayed or noisy measurements	Best for mildly nonlinear systems
UKF-RBF	Good, fast convergence	Moderate, controlled error	Moderate, limited robustness	Sigma point dispersion; unstable in high dimensions	General-purpose mid-noise environments
SSUKF-RBF	Excellent, very low error	Good, robust performance	Good, slow error growth	Extreme NLOS + high dynamic motion (slight increase)	Real-time indoor localization; mobile robotics
SSUKF-FA-RBF	Best, lowest error	Best, highly robust	Best, strong anti-noise ability	Risk of overfitting if poorly tuned	High-precision tasks; complex environment navigation

As indicated in Table 6, traditional filtering models such as IEKF-RBF, CKF-RBF, and EKF-RBF tend to experience significant error amplification or even divergence in NLOS and complex urban environments. These models are therefore more appropriate for settings characterized by low noise levels and simple spatial structures. The UKF-RBF model, due to its improved handling of nonlinearities, demonstrates moderate robustness and is better suited for positioning tasks under intermediate noise conditions. In contrast, both SSUKF-RBF and the proposed SSUKF-FA-RBF exhibit significantly enhanced robustness and stability in positioning accuracy across all tested environments. Notably, these models maintain low error margins even under adverse conditions, such as in NLOS scenarios and high-dynamic interference contexts. Among them, SSUKF-FA-RBF consistently delivers the highest accuracy and resilience, making it particularly well-suited for deployment in complex indoor navigation systems, unmanned autonomous platforms, and other high-precision positioning applications.

4.3 Discussion

This study systematically compares the positioning performance of various Kalman filter algorithms in integrated navigation systems [32], and introduces an improved SSUKF, along with a hybrid positioning model that integrates SSUKF with a FA-RBF neural network. Simulation experiments demonstrate that the proposed method offers significant advantages in positioning accuracy, robustness, and computational efficiency. These advantages are particularly evident under high measurement noise conditions, where the method exhibits strong stability and resistance to interference. Traditional UKFs estimate nonlinear system states by sampling sigma points derived from the statistical distribution of state variables. However, in high-dimensional nonlinear systems, the symmetric sampling strategy adopted by standard UKF often leads to sparsely distributed or divergent sigma points, which can result in filter divergence or the accumulation of estimation errors. To overcome this limitation, the SSUKF algorithm incorporates the SSUT, which enhances the distribution of sigma points by making them more representative and compact in high-dimensional spaces. The geometric structure of SSUT ensures that the sigma points better capture the underlying state distribution while maintaining computational tractability, thereby significantly reducing linearization errors. Experimental results confirm the effectiveness of the proposed

approach. The SSUKF achieves superior RMSE performance in position estimation, with a minimum RMSE of 0.1614 m-substantially lower than those of UKF (0.3371 m) and EKF (0.4271 m). In addition, SSUKF demonstrates high accuracy in velocity estimation, attaining a minimum RMSE of only 0.0501 m per second. These results validate the robustness and precision of SSUKF in handling high-noise and highly nonlinear navigation scenarios.

To further enhance the accuracy and generalization capability of the TDOA positioning method, this study employs the FA to optimize the param of the RBF neural network. Compared with commonly used optimization techniques such as GAs and PSO, FA operates based on a brightness-attraction mechanism that enables dynamic balancing between global exploration and local exploitation. This results in more flexible search trajectories and improved convergence behavior. The iterative multi-agent updates guided by brightness differences also allow FA to escape local optima effectively in complex, non-convex loss landscapes, thereby mitigating the risk of premature convergence. In contrast to GA, which relies on crossover and mutation operations, FA requires fewer control param and exhibits faster convergence rates, making it well-suited for real-time optimization tasks in dynamic environments. In high-dimensional continuous parameter spaces, FA demonstrates strong adaptability and precision, enabling effective tuning of key RBF network param, including the centers, weights, and widths. Experimental results confirm the effectiveness of this approach. The SSUKF-FA-RBF model consistently achieves the lowest RMSE and MAE across all tested standard deviation conditions. Under high-noise conditions, with a measurement standard deviation of 0.5 m, the model achieves an RMSE of only 0.127 m-significantly outperforming unoptimized RBF-based models such as EKF-RBF, which records an RMSE of 0.317 m. Furthermore, the error growth curve of the SSUKF-FA-RBF model remains smooth and stable, reflecting its strong robustness and reliability in noisy environments.

Despite the outstanding performance of the proposed SSUKF-FA-RBF model in simulation environments, several limitations remain with regard to real-world applications. In terms of data environments, the UWB TDOA dataset employed in this study reflects a typical indoor localization scenario characterized by relatively stable channel conditions. However, the model's adaptability to outdoor environments, particularly in cases involving frequent GNSS signal obstruction or dynamic signal switching, requires further empirical validation. Regarding scalability and computational cost, although the FA demonstrates faster convergence than traditional methods such as GAs and PSO, real-time iterative optimization in large-scale multi-agent systems-such as vehicular networks or robotic swarms-may still impose considerable computational burdens. From the perspective of input adaptability, the current model is specifically designed for TDOA signal features. When extended to other signal modalities such as Wi-Fi, ultrasound, or vision-based systems, input features would require redefinition, and the neural network architecture might need structural adjustments to maintain performance. In terms of hardware deployment, the model is designed for execution on devices with moderate computational capabilities, such as edge computing nodes or embedded systems. For highly resource-constrained or low-power devices, model compression or lightweight adaptation strategies would be essential to enable efficient deployment. This study introduces the SSUKF filter by integrating the SSUT into the traditional UKF framework, thereby significantly improving filtering accuracy and stability under nonlinear and high-noise conditions. Furthermore, the incorporation of an FA-optimized RBF neural network enhances the overall performance of the TDOA localization system, enabling it to maintain low positioning errors even in complex and noisy environments. Compared with existing methods, the proposed approach not only delivers substantial improvements in accuracy and robustness but also offers favorable computational efficiency, underscoring its practical potential and engineering applicability in real-time navigation and localization systems.

5 Conclusion

This study compares the positioning performance of various KF algorithms within an integrated navigation system. The results demonstrate that the proposed SSUKF algorithm achieves outstanding positioning accuracy. Specifically, the mean position error of SSUKF is 0.3172 m, which is significantly lower than those of other evaluated algorithms. Additionally, the RMSE of SSUKF reaches 0.1614 m, further confirming its superior precision. These results indicate that SSUKF effectively enhances positioning accuracy by reducing error fluctuations and improving overall estimation stability. In velocity estimation, SSUKF also outperforms comparison algorithms, with a mean velocity error of 0.0103 m per second and a correspondingly lower RMSE, highlighting its advantage in high-precision dynamic state estimation. From a computational perspective, SSUKF achieves a processing time of 7.69 seconds, underscoring its efficiency in reducing computational load and supporting real-time applications. Following optimization of the TDOA method, the combined models SSUKF-RBF and SSUKF-FA-RBF exhibit excellent positioning accuracy and robustness under varying measurement noise levels. Particularly under high measurement standard deviations, SSUKF-FA-RBF outperforms other models, maintaining superior accuracy and exhibiting a slower error growth rate as noise increases. Across all test conditions, SSUKF-FA-RBF consistently achieves high accuracy, precision, and area under the curve metrics. Notably, it demonstrates exceptional robustness and stability in both low-error and high-error scenarios, validating its effectiveness for practical positioning tasks in complex and noisy environments.

Although this study has demonstrated the high accuracy and robustness of the SSUKF-FA-RBF model

for indoor TDOA localization, several limitations remain. First, the current model does not incorporate multi-sensor fusion mechanisms. In practical applications such as GPS-denied environments (e.g., underground spaces, tunnels, or dense urban canyons) and scenarios involving rapid dynamic changes (e.g., complex urban traffic or moving obstacles), reliance on a single sensor modality may compromise system stability and accuracy. Second, the model has not yet been extended to integrate heterogeneous information sources such as visual sensors or LiDAR, nor has it been adapted for six-degree-of-freedom (6-DoF) pose estimation or multi-agent cooperative localization. These limitations restrict its applicability in broader global navigation and large-scale mobile system contexts. Future research directions may include the development of multi-source fusion frameworks that combine GNSS, IMUs, UWB, and vision-based sensors to improve adaptability and resilience in complex environments. Moreover, implementing adaptive estimation techniques with dynamic weighting schemes could enhance system robustness against abrupt interferences or sensor failures. Extending the algorithm to support 6-DoF pose estimation, enabling simultaneous position and orientation determination, as well as investigating cooperative localization strategies for multi-agent systems, would significantly benefit applications such as swarm robotics and intelligent vehicle fleets.

Funding

This work was supported by Science and Technology Program of Zhejiang Provincial Department of Transportation under Grant 2024012, “Pioneer” and “Leading Goose” R & D Program of Zhejiang under Grant 2023C03154.2024 ZheJiang Institute of Communications Talent Introduction Plan Project.

Data availability statement

All data generated or analysed during this study are included in this article.

Conflict of interest

The authors declare that they have no competing interests.

References

[1] Gao W, Zhou W, Tang C, et al. High-precision services of BeiDou navigation satellite system (BDS): Current state, achievements, and future directions. Satellite Navigation, 2024, 5(1): 20. https://doi.org/10.1186/s43020-024-00143-8

[2] Xiao Y, Wang Z, Chao N, et al. Gravity field recovery of inter-satellite links between Beidou navigation satellite system (BDS) and LEO based on geodesy and time reference in space (GETRIS). Advances in Space Research, 2024, 73(12): 5889-5909. https://doi.org/10.1016/j.asr.2024.03.025

[3] Zhang S, Tu R, Gao Z, et al. LEO-enhanced GNSS/INS tightly coupled integration based on factor graph optimization in the urban environment. Remote Sensing, 2024, 16(10): 1782. https://doi.org/10.3390/rs16101782

[4] Zhang L, Lou Y, Song W, et al. Performance enhancement of PPP/SINS tightly coupled navigation based on improved robust maximum correntropy kalman filtering. Advances in Space Research, 2024, 74(5): 2078-2091. doi: 10.1016/j.asr.2024.05.072

[5] Pang S, Zhang B, Lu J, et al. Application of IMU/GPS integrated navigation system based on adaptive unscented kalman filter algorithm in 3D positioning of forest rescue personnel. Sensors, 2024, 24(18): 5873. doi: 10.3390/s24185873

[6] Chen W, Wang T, Yao Z, et al. Analysis of the gain factors of 5G-assisted BDS RTK positioning in urban environments. Satellite Navigation, 2024, 5(1): 28. https://doi.org/10.1186/s43020-024-00149-2

[7] Li F, Tu R, Geng F, et al. Combined BDS/5G seamless positioning scheme based on joint switching strategy of satellite elevation angle and CNR in complex urban environments. Measurement Science and Technology, 2024, 35(12): 126307. https://doi.org/10.1088/1361-6501/ad7a1e

[8] Liaquat S, Faizan M, Chattha J N, et al. A framework for preventing unauthorized drone intrusions through radar detection and GPS spoofing. Ain Shams Engineering Journal, 2024, 15(5): 102707. https://doi.org/10.1016/j.asej.2024.102707

[9] Chen W, Jing Y, Zhao S, et al. A distributed collaborative navigation strategy based on adaptive extended kalman filter integrated positioning and model predictive control for global navigation satellite system/inertial navigation system dual-robot. Remote Sensing, 2025, 17(4): 721. https://doi.org/10.3390/rs17040721

[10] Park G. Optimal vehicle position estimation using adaptive unscented Kalman filter based on sensor fusion. Mechatronics, 2024, 99(1): 103144. https://doi.org/10.1016/j.mechatronics.2024.103144

[11] Yin Y, Zhang J, Guo M, et al. Sensor fusion of GNSS and IMU data for robust localization via smoothed error state Kalman filter. Sensors, 2023, 23(7): 3676. https://doi.org/10.3390/s23073676

[12] Wu Q, Li C, Shen T, et al. Improved adaptive iterated extended kalman filter for GNSS/INS/UWB-integrated fixed-point positioning. CMES-Computer Modeling in Engineering & Sciences, 2023, 134(3): 1. https://doi.org/10.32604/cmes.2022.020545

[13] Yuan Y, Li F, Chen J, et al. An improved Kalman filter algorithm for tightly GNSS/INS integrated navigation system. Math. Biosci. Eng, 2024, 21(1): 963-983. https://doi.org/10.3934/mbe.2024040

[14] Neusypin K, Kupriyanov A, Maslennikov A, et al. Investigation into the nonlinear Kalman filter to correct the INS/GNSS integrated navigation system. GPS Solutions, 2023, 27(2): 91.

https://doi.org/10.1007/s10291-023-01433-5
[15] Zhang T, Guo S, Fan L, et al. Improving BeiDou global navigation satellite system (BDS-3)-derived station coordinates using calibrated satellite antennas and station inter-system translation param. Remote Sensing, 2025, 17(3): 1. https://doi.org/10.3390/rs17030510
[16] Fu X, Zhao K, Sun Y, et al. A novel cascading partial ambiguity resolution method of BDS triple-frequency with inertial aiding for kinematic-to-kinematic relative positioning. Measurement Science and Technology, 2024, 36(1): 016316. https://doi.org/10.1088/1361-6501/ad86e4
[17] Cao Y, Lian W, Yang J, et al. Design of high-precision displacement safety monitoring and three-dimensional spatial alarm system for Beidou based on intelligent algorithms. Measurement: Sensors, 2024, 33(1): 101099. https://doi.org/10.1016/j.measen.2024.101099
[18] Khodarahmi M, Maihami V. A review on Kalman filter models. Archives of Computational Methods in Engineering, 2023, 30(1): 727-747. https://doi.org/10.1007/s11831-022-09815-7
[19] Bai Y, Yan B, Zhou C, et al. State of art on state estimation: Kalman filter driven by machine learning. Annual Reviews in Control, 2023, 56(1): 100909. https://doi.org/10.1016/j.arcontrol.2023.100909
[20] Feng S, Li X, Zhang S, et al. A review: State estimation based on hybrid models of Kalman filter and neural network. Systems Science & Control Engineering, 2023, 11(1): 2173682. https://doi.org/10.1080/21642583.2023.
[21] Rosafalco L, Conti P, Manzoni A, et al. EKF-SINDy: Empowering the extended Kalman filter with sparse identification of nonlinear dynamics. Computer Methods in Applied Mechanics and Engineering, 2024, 431(1): 117264. https://doi.org/10.1016/j.cma.2024.117264
[22] Takyi-Aninakwa P, Wang S, Liu G, et al. Enhanced extended-input LSTM with an adaptive singular value decomposition UKF for LIB SOC estimation using full-cycle current rate and temperature data. Applied Energy, 2024, 363(1): 123056. https://doi.org/10.1016/j.apenergy.2024.123056
[23] Moradi-Sarvestani S, Jooshaki M, Fotuhi-Firuzabad M, et al. Incorporating direct load control demand response into active distribution system planning. Applied Energy, 2023, 339(2): 120897. https://doi.org/10.1016/j.apenergy.2023.120897
[24] Peng S, Zuo J, Xu W, et al. Fractional moments based adaptive scaled unscented transformation for probabilistic power flow of AC-DC hybrid grids. IEEE Transactions on Power Systems, 2024, 39(5): 6249-6262. https://doi.org/10.1109/TPWRS.2024.3364674
[25] Wang L, Chen T, Zou C. The TSCR method for precision estimation of ill-posed mixed additive and multiplicative random error model. Communications in Statistics-Simulation and Computation, 2024, 53(9): 4581-4595. https://doi.org/10.1080/03610918.2022.2154801
[26] Zhang X, Kang J, Yu H. Intelligent Navigation system based on big data traffic system. scalable computing: Practice and experience, 2024, 25(2): 1. https://doi.org/10.12694/scpe.v25i2.2654
[27] Okada T, Dong S, Kuzuno R, et al. State observer of multibody systems formulated using differential algebraic equations. Multibody System Dynamics, 2024, 1(1): 1-31. https://doi.org/10.1007/s11044-024-09995-z
[28] Tu C, Cui X, Liu G, et al. Parameterized TDOA: TDOA estimation for mobile target localization in a time-division broadcast positioning system. IEEE Internet of Things Journal, 2025, 1(1): 1-1. https://doi.org/10.1109/JIOT.2025.3554528
[29] Wang J. Construction of student performance prediction model based on data mining and optimized RBF neural network. Informatica, 2024, 48(17): 1. doi: 10.31449/inf.v48i17.6516
[30] Karim R, Hasan M, Kundu A K, et al. LP SVM with a novel similarity function outperforms powerful LP-QP-Kernel-SVM considering efficient classification. Informatica, 2023, 47(8): 1. https://doi.org/10.31449/inf.v47i8.4767
[31] Constantinopoulos C, Likas A. An incremental training method for the probabilistic RBF network. IEEE Transactions on Neural Networks, 2024, 17(4): 966-974. https://doi.org/10.1109/TNN.2006.875982
[32] Hamza V. Low-cost GNSS receivers for geodetic monitoring purposes. Informatica, 2023, 47(4): 1. https://doi.org/10.31449/inf.v47i4.5422